PCCP

Accepted Manuscript

ROYAL SOCIETY OF CHEMISTRY

www.rsc.org/pccp

Collision Cross Section Measurements for Biomolecules within a High-Resolution FT-ICR Cell: Theory

Dan Guo,[1] Yi Xin,[1] Dayu Li,[2] Wei Xu[1*]

[1]School of Life Science, Beijing Institute of Technology, Beijing 100081, China

[2]College of Information Science and Engineering, Northeastern University, Shenyang 110819, China

*Corresponding Author:
Wei Xu
School of Life Science
Beijing Institute of Technology
Haidian, Beijing, 100081, China
Email: weixu@bit.edu.cn
Phone: +86-10-68918123

Abstract:

In this study, an energetic hard-sphere ion-neutral collision model was proposed to bridge-link ion collision cross section (CCS) with the image current collected from a high-resolution Fourier transform ion cyclotron resonance (FT-ICR) cell. By investigating the nonlinear effects induced by high-order electric fields and image charge forces, the energetic hard-sphere collision model was validated through experiments. Suitable application regions for the energetic hard-sphere collision model, as well as for the conventional Langevin and hard-sphere collision models, were also discussed. The energetic hard-sphere collision model was applied in the extraction of ion CCSs from high-resolution FT-ICR mass spectra. Discussions in the present study also apply to FT-Orbitraps and FT-quadrupole ion traps.

Key words: collision cross section, energetic hard-sphere ion-neutral collision model, FT-ICR, Langevin collision model, hard-sphere collision model

1. Introduction

Ion-neutral collision is an important phenomenon in FT-ICR cells, which closely relates to ion cooling, collision induced dissociation (CID) and mass resolution of the system.[1-4] Ion-neutral collisions could remove excess kinetic energy of ions, and cool ions to the center of an ICR cell after ion injection or excitation.[5-8] Collisional damping of ion motions in an ICR cell shortens the duration of detectable ion transient signal, which results in lower mass resolution and broadening of the mass spectrum peaks.[3, 9, 10] On the other hand, ion-neutral collisions have also been utilized to characterize the size of an ion (collision cross section, CCS), since ion-neutral collision rate is a function of the CCS of an ion under controlled conditions.[11-16] A direct relationship between CCS and the ion motion decay profile or the spectrum peak shape is critical in ion CCS measurements. Therefore, a realistic and accurate theoretical ion-neutral collision model is essential in the understanding of ion-neutral collision effects and performing ion CCS measurements.

Conventionally, there are two collision models, the Langevin collision model and the hard-sphere collision model. The Langevin collision model treats an ion as a point charge, a neutral molecule as an electric dipole induced by the ion.[10, 12, 17] The Langevin collision model is a good approximation of low energy collisions between neutral molecules and small ions, whose hard-sphere CCSs are much smaller than their Langevin CCSs. For an ion of larger physical radius and higher velocity, the Langevin CCS would be smaller than the hard-sphere CCS. In this case, the hard-sphere collision model is more accurate.[18] Although the Langevin and the

hard-sphere collision models have been successfully applied in the characterization of ion damping motions within ICR cells, as well as in quadrupole ion traps,[19, 20] there are limitations in describing high energy ion-neutral collisions,[21, 22] especially in modern high-resolution FT-ICR systems.[23-25] By proposing that ion-neutral collisions scatter ions out of a coherent packet, Yang et al. realized the CCS measurement of crown ether ions in a 4.7 T FT-ICR instrument.[11]

In this work, a new ion-neutral collision model for energetic ions in high-resolution FT-ICR instruments (higher magnetic fields and bigger FT-ICR cell radius), the energetic hard-sphere collision model was proposed and studied systematically in terms of: 1) performing a comparison study of the Langevin, the hard-sphere and the energetic hard-sphere collision models with respect to image current decay profiles and spectrum line shapes; 2) discussing suitable application conditions for these three collision models; 3) validating the energetic hard-sphere collision model with experimental results through the investigation of nonlinear effects. It is found that the Langevin collision model is almost never appropriate for describing collisions of ions during detection events in modern FTICR instrumentation. With stronger magnetic fields and larger ICR cell radiuses in high-resolution FT-ICR instruments, the energetic hard-sphere collision model would be a better description of ion-neutral collisions. This energetic hard-sphere collision model was then used in experiments for the CCS measurements of biomolecules in a high-resolution FT-ICR instrument.[26]

2. Ion-neutral collision modeling

To obtain CCS of an ion in a Fourier transform mass analyzer, FT-ICR for instance, an ion-neutral collision model is essential to bridge the measured image currents with ion CCSs. In different instruments and at different operation conditions, ions may experience different types of ion-neutral collisions. Well studied in literatures,[17,18] the Langevin and the hard-sphere collision models were briefly discussed here, and details about the derivations could be found in the Supporting Information.

The Langevin collision model. The Langevin collision model treats an ion as a point charge with no dimensions that induces a dipole moment in the neutral collision partner, and ion-neutral collision is a result of ion-dipole attraction.[27] CCS for an ion (σ) is inversely proportional to velocity of the ion:

$$\sigma = \frac{q\sqrt{\frac{\alpha(M+m)}{mM}}}{2\,v\,\varepsilon_0} \tag{1}$$

where v is ion velocity; α is the ion-neutral polarizability; ε_0 is the permittivity of vacuum; M is the mass of the neutral molecule; m is mass of the ion; q is the charge the ion possesses. As a good description of low energy collisions between small ions and neutrals, the Langevin collision model results in exponential decay of ion velocity (see Supporting Information for details).

$$v = v_0 e^{-t\,c_1} \tag{2}$$

where v_0 is ion initial velocity; $c_1 = \frac{q\sqrt{\frac{\alpha(M+m)}{mM}}}{2\varepsilon_0}\frac{p}{Tk}\frac{M}{m+M}$; p is pressure and T is temperature. Since ion velocity is in direct proportion with measured image current,[28,

[29] the signal intensity also decays exponentially. However, collision probability is independent of ion velocity, and ion CCS could not be extracted from ICR signals if the Langevin collision model is dominant in experiments.

The hard-sphere collision model. The hard-sphere collision model is a better description for ions possessing more kinetic energies and/or higher masses.[18] In the hard-sphere collision model, ion CCS is a constant, and collision probability is proportional to ion velocity. If an ion undergoes multiple collisions before fragmentation or dephasing, ion-neutral collision can still be treated as a frictional damping force, which is proportional to the square of ion velocity. It could be found that the resulting time-domain ICR signal has the form (see Supporting Information for details)

$$v = \frac{v_0}{t\, v_0\, c_2 + 1} \tag{3}$$

in which $c_2 = \sigma \frac{p}{Tk} \frac{M}{m+M}$. Different from the Langevin collision model, the corresponding frequency-domain spectrum of the hard-sphere collision model doesn't have a concise analytical expression (see Supporting Information for details).

The energetic hard-sphere collision model. Conventional collision models may no longer be accurate to describe ion-neutral collisions in modern FT-ICR instruments, where higher magnetic field and larger ICR cells are typically applied to achieve higher mass resolution. In an ICR cell, speed of an ion after excitation is proportional to magnetic field strength and post excitation cyclotron radius,[1] and is typically high in modern FT-ICR instruments. Table 1 shows typical ion kinetic energies in the laboratory reference frame after excitation for the present experiments (briefly, 9.4 T,

ICR cell inner diameter 94 mm, details in ref[26]), and maximum exchange energy was calculated under the assumption of 100% inelastic collision, for which the total kinetic energy loss *(⊿KE)* is

$$\Delta KE \cong KE \times \frac{2M}{m} \quad (4)$$

in which *KE* is the kinetic energy in the laboratory reference frame of the ion before collision. Here, we assume the mass and initial *KE* of the ion are much higher than those of neutral molecules.

A small ion would undergo fragmentation under such energetic collisions (shown in Table 1). If a single collision is able to dephase (or fragment) the ion from a spatially coherent ion packet, ion number (*N*) change in the ion packet during excitation would follow,[11]

$$dN = -Nnv\sigma dt \quad (5)$$

in which *n* is the neutral density, and *n* = *p/kT* according to the ideal gas law. By ignoring other effects (space charge, field imperfection, resistive coupling between the ion and detection circuit, etc.), ion speed will be constant before ion-neutral collisions. Thus,

$$N(t) = N_0 e^{-c_3 t} \quad (6)$$

in which c_3 is the decay factor, *nvσ*. Different from the Langevin and the hard-sphere collision models, ion-neutral collisions result in ion number decrease in a coherent ion packet for the energetic hard-sphere collision model,[11] instead of ion cyclotron radius decrease.

Comparison of the three collision models. Ion-neutral collisions have effects

on both time-domain image current decay profiles and the corresponding frequency-domain spectrum peak shapes. Figure 1 shows the image current decay profiles and their corresponding frequency-domain spectrum peak shapes for a small ion (tetramethylammonium, m/z 74.1, hard-sphere collision cross section 107.4 Å^2 [30]) and a larger ion (angiotensin I, m/z 433, hard-sphere collision cross section 474 Å^2 [31]) using different collision models. Signal decay under the Langevin collision model is hardly noticeable in 5 seconds (magnetic field strength 7 T and ion cyclotron radius 20 mm). As shown in Figure 1, energetic hard-sphere collisions normally lead to faster image current decays and broader spectrum peak widths. That is because the reduced momentum in a single collision is proportional to $\frac{M\,m\,v}{m+M}$ under Langevin and hard-sphere collisions, while proportional to mv in an energetic hard-sphere collision. In all three collision models, the background gas pressure has significant effects on signal decay rates (c_1, c_2 and c_3 in Equation 2, 3 and 6, respectively). Higher pressure leads to faster signal decay and shorter image current signal detectable duration. It is found in experiments that the line width has a close to linear relationship with respect to buffer gas pressure under the energetic hard-sphere collision conditions; while a nonlinear correlation under the hard-sphere collision conditions.[11] As shown in Equation (1), ion CCS is *KE* dependent in the Langevin collision model. However, in both hard-sphere and energetic hard-sphere collision models, ion CCS is assumed to be a constant, which reflects the physical dimensions of an ion. It should also be noticed that the energetic hard-sphere collision model results in the widely-observed Lorentzian FT-ICR line shapes (Equation 6, Figure 1b

and 1d) without requiring Langevin collisions.

Suitable application regions of the three collision models. One of the potential applications of ion-neutral collision modeling is to provide a theoretical basis for the measurement of ion CCSs. The successful extraction of ion CCSs from FT-ICR image current signals highly depends on the proper selection of an ion-neutral collision model. Knowing the application conditions of different collision models contributes to build reliable experimental methods to measure the CCS of an ion. In general, the Langevin collision model applies to low-energy ions, whose hard-sphere CCSs are small comparing to their Langevin CCSs; while the hard-sphere collision model applies to large ions, whose polarization forces with neutral molecules can be ignored. However, the selection of ion-neutral collision model is complicated, which depends on physical property of the ion and the ICR cell, as well as operation conditions of the FT-ICR instrument. As an example, Figure 2 shows the suitable application regions of the three ion-neutral collision models for cytochrome C and ubiquitin ions at different FT-ICR operation conditions, including magnetic field strength and ion excitation radius. Solid lines in Figure 2 indicate when the hard-sphere CCSs become larger than the Langevin CCSs. The hard-sphere CCSs for cytochrome C ions were taken from ion mobility measurements (Note: the CCSs obtained from ion mobility may not be the true CCSs in hard-sphere or energetic hard-sphere collision conditions, in which cases the ion *KE*s may be much higher than those in ion mobility measurements).[32] Discrimination of energetic hard-sphere collision model from hard-sphere collision model depends on a threshold *KE* that is required to dephase (or fragment) the ion

from the ion packet. The threshold *KE* is associated with the chemical properties of ions, such as bond energy and spatial structure of every specific ion, which needs experimental measurements. In this study, assumptions were made for ions on this threshold *KE*, and effects of this *KE* were also discussed as shown in Figure 2. The dashed lines in Figure 2 separate the energetic hard-sphere collision model regions from those of the hard-sphere collision model. A 5000 eV is assumed to be the threshold *KE* for cytochrome C ions in Figure 2a, and Figure 2b shows the effects of this threshold *KE* for ubiquitin (7+) ions (the hard-sphere CCS of ubiquitin 7+ was taken from ref[33]). In modern high-resolution FT-ICR instruments with magnetic fields typically stronger than 4 Tesla, the Langevin collision model is hardly applicable throughout the course of signal detection, especially for biomolecules with larger hard-sphere CCSs. For the FT-ICR instrument used in ref[26] (9.4 T, ion excitation radius >18 mm), the energetic hard-sphere collision model would apply for most ions tested in experiments, such as organic, peptide and small protein ions.

3. Nonlinear effects and verification of the energetic hard-sphere collision model

The major difference between the energetic hard-sphere collision model and the other two collision models (the Langevin and the hard-sphere collision models) is that: cyclotron radius of the ion coherent packet will not decrease due to ion-neutral collisions for the energetic hard-sphere collision model; while cyclotron radius of the ion coherent packet decreases as shown in Equation 2 and 3 for the other two collision models. Since nonlinear effects would cause ion motion frequency shift at different cyclotron radius,[34-36] nonlinear effects within the FT-ICR cell were studied and

utilized to verify that energetic hard-sphere collisions are dominant in experiments.[26]

In this work, nonlinear effects caused by the high-order electric fields were investigated first. In the FTICR cell used in experiments,[26] there exist high-order electric fields besides the quadrupole electric field. In an ICR cell, the ion motion equation can be written as,

$$mr\omega^2 = qB\omega r + q\frac{\partial\phi(r,z)}{\partial r} \tag{7}$$

in which r is ion motion radius, ω is ion motion angular frequency, B is magnetic field strength, $\phi(r,z)$ is the summation of high-order electric fields, and[37]

$$\phi(r,z) = -V\left(A_2\frac{r^2-2z^2}{2r_0^2} + A_3\frac{3r^2z-2z^3}{2r_0^3} + A_4\frac{3r^4-24r^2z^2+8z^4}{8r_0^4} + A_5\frac{15r^4z-40r^2z^3+8z^5}{8r_0^5} + A_6\frac{5r^6-90r^4z^2+120r^2z^4-16z^6}{16r_0^6}\right) \tag{8}$$

where V is the electric trapping potential, A_n is the coefficients of high-order field components and r_0 is inner radius of the ICR cell. At the central plane of the trap, z = 0

$$\frac{\partial\phi(r,z)}{\partial r}\Big|_{z=0} = -V(A_2\frac{2r}{2r_0^2} + A_4\frac{12r^3}{8r_0^4} + A_6\frac{30r^5}{16r_0^6}) \tag{9}$$

Substituting Equation (9) into Equation (7), ion motion equation becomes,

$$mr\omega^2 = qB\omega r - qV(A_2\frac{2r}{2r_0^2} + A_4\frac{12r^3}{8r_0^4} + A_6\frac{30r^5}{16r_0^6}) \tag{10}$$

Solve the above equation; the modified ion cyclotron motion frequency could be obtained as

$$\omega = \frac{\omega_c}{2} + \frac{\sqrt{q^2B^2-4qmV(A_2\frac{2}{2r_0^2}+A_4\frac{12r^2}{8r_0^4}+A_6\frac{30r^4}{16r_0^6})}}{2\,m} \tag{11}$$

ω_c is the "unperturbed" ion cyclotron frequency.

Besides high-order electric fields, image charges induced on the detection electrodes would generate an electric field, which would also cause nonlinear effects

on ion motion. The radial force generated by the image charge can be written as[35]

$$F = -\frac{1}{2}q\nabla\varphi = 0.5\frac{Kqn}{r_0}\left(\frac{\xi_1 2r}{r_0^2} + \frac{\xi_2 4r^3}{r_0^4}\right) \quad (12)$$

where K is the Coulomb constant, φ is the potential induced by image charge, and for an infinite long cylinder trap, $\xi_1 = 1.0027$ and $\xi_2 = 1.0009$.[35] When considering this force, ion motion equation becomes:

$$mr\omega^2 = qB\omega r - 0.5\frac{Kqn}{r_0}\left(\frac{\xi_1 2r}{r_0^2} + \frac{\xi_2 4r^3}{r_0^4}\right) \quad (13)$$

The modified ion cyclotron motion frequency could be obtained by solving Equation (13),

$$\omega = \frac{\omega_c}{2} + \frac{\sqrt{q^2B^2 - 2qm\frac{Kqn}{r_0}\left(\frac{\xi_1 2}{r_0^2} + \frac{\xi_2 4r^2}{r_0^4}\right)}}{2\,m} \quad (14)$$

Nonlinear effects on ion motion frequency and line shape. Figure 3a shows the nonlinear effects on ion cyclotron motion frequency. Ion motion frequency will be shifted up with the existence of -20% octopole and 10% dodecapole electric fields. Larger frequency shifts could be observed at larger ion motion radiuses. Ion motion frequency will be shifted down by the image charge induced by $1.2*10^6$ ions. When considering both high-order field and image charge effects, ion motion frequency shift is complicated, which increases first with increased ion motion radius due to high-order field effects and then decreases due to the domination of image charge effects. The fact that ion frequency varies at different cyclotron radiuses will broaden the spectrum for both the Langevin and the hard-sphere collision models. Figure 3b plots the corresponding spectrum line shape when the hard-sphere collision model is dominant. Motion radius of an ion coherent packet is a constant in the energetic hard-sphere collision model. Therefore, there will be no frequency shift or spectrum

peak shape distortion under the condition of the energetic hard-sphere collision model.

Experimental section. Experiments were performed in a home-built FT-ICR instrument whose ICR cell consists of 7 cylindrical 94 mm inner diameter segments.[25] Ubiquitin was purchased from Sigma Aldrich (St. Louis, MO, USA). Samples were used without further purification. Electrosprayed samples were diluted to 1 μm/L in methanol/water 1:1 v/v with 0.1% formic acid. Transient image current data were collected for 6.115 s with 8388608 data points. Data were further processed with Matlab (MathWorks Inc.) without zero filling.

Experimental results. Image charge forces and high-order fields may cause ion cyclotron frequency shift at different cyclotron radiuses, which can be used as a method to discriminate energetic hard-sphere collisions from Langevin and hard-sphere collisions. It was found from experiments that ion cyclotron frequency varies with ion cyclotron radius. Figure 4a plots the Fourier transform spectrum of one-second-long time-domain signals of ubiquitin ions (8+) at 30%, 40%, 50% and 60% excitation radiuses, respectively. As shown in Figure 4b, the frequency of ubiquitin (8+) ions increases with larger cyclotron radius, a result of the high-order electric field effects; and then decreases after the ion excitation radius is larger than 50%, which is due to the domination of image charge force effects. Experimental results suggest that: 1) there exist nonlinear effects from both high-order electric fields and image charge forces in the ICR cell; 2) no obvious line shape distortion was observed, thus energetic hard-sphere collisions were dominant in experiments. Furthermore, image

current of ubiquitin ions was recorded for a longer period (four seconds), and the time-domain signal was Fourier transformed at every one second as shown in Figure 5. It is found that although amplitude of the image current will decrease with time, ion cyclotron frequency does not shift, which further confirms that the energetic hard-sphere collision is dominant in the modern high-resolution FT-ICR system used in our experiments.[26]

4. Conclusions

In this work, the relationship between ion CCSs and the corresponding image current decay characteristics were established for modern high-resolution FT-ICR instruments. Besides discussing suitable application conditions of the Langevin and the hard-sphere ion-neutral collision models, the energetic hard-sphere collision model was developed and discussed for modern high-resolution FT-ICR instruments. By investigating nonlinear effects, it is found that the energetic hard-sphere collision model is more suitable under experimental conditions as in ref[26]. Theoretical results found in this work were then utilized in experiments for the measurements of ion CCSs in an FT-ICR cell.

Acknowledgements

We are grateful for the help from Prof. Alan Marshall of Florida State University. This work was supported by National Natural Science Foundation of China (21205005, 21475010), 1000 plan and MOST Instrumentation Program of China (2011YQ0900502).

References

1. Marshall, A. G.; Hendrickson, C. L.; Jackson, G. S., Fourier transform ion cyclotron resonance mass spectrometry: a primer. *Mass spectrometry reviews* **1998,** 17, (1), 1-35.
2. Laskin, J.; Futrell, J. H., Collisional activation of peptide ions in FT‐ICR mass spectrometry. *Mass spectrometry reviews* **2003,** 22, (3), 158-181.
3. Marshall, A. G.; Comisarow, M. B.; Parisod, G., Relaxation and spectral line shape in Fourier transform ion resonance spectroscopy. *The Journal of Chemical Physics* **1979,** 71, (11), 4434-4444.
4. Cooks, R. G., Special feature: Historical. Collision-induced dissociation: Readings and commentary. *Journal of Mass Spectrometry* **1995,** 30, (9), 1215-1221.
5. Speir, J. P.; Gorman, G. S.; Pitsenberger, C. C.; Turner, C. A.; Wang, P. P.; Amster, I. J., Remeasurement of ions using quadrupolar excitation Fourier transform ion cyclotron resonance spectrometry. *Analytical chemistry* **1993,** 65, (13), 1746-1752.
6. Schweikhard, L.; Guan, S.; Marshall, A. G., Quadrupolar excitation and collisional cooling for axialization and high pressure trapping of ions in Fourier transform ion cyclotron resonance mass spectrometry. *International journal of mass spectrometry and ion processes* **1992,** 120, (1), 71-83.
7. Williams, E. R.; Henry, K. D.; McLafferty, F. W., Multiple remeasurement of ions in Fourier-transform mass spectrometry. *Journal of the American Chemical Society* **1990,** 112, (17), 6157-6162.
8. Guan, Z.; Hofstadler, S. A.; Laude Jr, D. A., Remeasurement of electrosprayed proteins in the trapped ion cell of a Fourier transform ion cyclotron resonance mass spectrometer. *Analytical chemistry* **1993,** 65, (11), 1588-1593.
9. Ridge, D. P.; Beauchamp, J. L., The interaction of ions with nonpolar neutrals: The collision broadening of ion cyclotron resonance lines of ions in hydrogen and methane. *The Journal of Chemical Physics* **1976,** 64, (7), 2735-2746.
10. Beauchamp, J. L., Theory of Collision‐Broadened Ion Cyclotron Resonance Spectra. *The Journal of Chemical Physics* **1967,** 46, (4), 1231-1243.
11. Yang, F.; Voelkel, J. E.; Dearden, D. V., Collision cross sectional areas from analysis of fourier transform ion cyclotron resonance line width: a new method for characterizing molecular structure. *Analytical chemistry* **2012,** 84, (11), 4851-4857.
12. Wobschall, D.; Graham Jr, J. R.; Malone, D. P., Ion cyclotron resonance and the determination of collision cross sections. *Physical Review* **1963,** 131, (4), 1565.
13. Wobschall, D.; Fluegge, R. A.; Graham, J. R., Collision Cross Sections of Hydrogen and Other Ions as Determined by Ion Cyclotron Resonance. *The Journal of Chemical Physics* **1967,** 47, (10), 4091-4094.
14. Covey, T.; Douglas, D., Collision cross sections for protein ions. *Journal of the American Society for Mass Spectrometry* **1993,** 4, (8), 616-623.
15. Clemmer, D. E.; Jarrold, M. F., Ion mobility measurements and their applications to clusters and biomolecules. *Journal of Mass Spectrometry* **1997,** 32, (6), 577-592.
16. Buttrill Jr, S. E., Measurement of Ion-Molecule Reaction Rate Constants Using Ion Cyclotron Resonance. *The Journal of Chemical Physics* **1969,** 50, (10), 4125-4132.
17. Langevin, P., A fundamental formula of kinetic theory. *Annales de Chimie et de Physique* **1905,** 5, (0365-1444), 245-288.
18. Guan, S.; Li, G.-Z.; Marshall, A. G., Effect of ion-neutral collision mechanism on the trapped-ion

equation of motion: a new mass spectral line shape for high-mass trapped ions. *International journal of mass spectrometry and ion processes* **1997,** 167, 185-193.

19. He, M.; Guo, D.; Feng, Y.; Xiong, X.; Zhang, H.; Fang, X.; Xu, W., Realistic modeling of ion-neutral collisions in quadrupole ion traps. *Journal of Mass Spectrometry* **2014**.

20. He, M.; Guo, D.; Chen, Y.; Xiong, X.; Fang, X.; Xu, W., Ion Collision Cross Section Measurements in Quadrupole Ion Traps Using a Time-frequency Analysis Method. *Analyst*.

21. Riegner, D. E.; Laude Jr, D. A., Collision-mediated axial ejection of radially excited ions as a mass-dependent ion loss mechanism in Fourier transform ion cyclotron resonance mass spectrometry. *International journal of mass spectrometry and ion processes* **1992,** 120, (1), 103-116.

22. Arkin, C. R.; Laude, D. A., Collision induced ion ejection in an FTICR trapped-ion cell. *Journal of the American Society for Mass Spectrometry* **2005,** 16, (3), 422-430.

23. Nagornov, K. O.; Gorshkov, M. V.; Kozhinov, A. N.; Tsybin, Y. O., High-Resolution Fourier Transform Ion Cyclotron Resonance Mass Spectrometry with Increased Throughput for Biomolecular Analysis. *Analytical chemistry* **2014,** 86, (18), 9020-9028.

24. Huang, Y. L.; Pasatolic, L.; Guan, S. H.; Marshall, A. G., COLLISION-INDUCED DISSOCIATION FOR MASS-SPECTROMETRIC ANALYSIS OF BIOPOLYMERS - HIGH-RESOLUTION FOURIER-TRANSFORM ION-CYCLOTRON RESONANCE MS(4). *Analytical chemistry* **1994,** 66, (24), 4385-4389.

25. Kaiser, N. K.; Savory, J. J.; McKenna, A. M.; Quinn, J. P.; Hendrickson, C. L.; Marshall, A. G., Electrically Compensated Fourier Transform Ion Cyclotron Resonance Cell for Complex Mixture Mass Analysis. *Analytical chemistry* **2011,** 83, (17), 6907-6910.

26. Mao, L.; Chen, Y.; Xu, W., Extracting Biomolecule Collision Cross Sections from the Line Width of High-resolution FT-ICR Mass Spectrometry. *submitted*.

27. Su, T.; Bowers, M. T., Ion-polar molecular collisions: the average quadrupole orientation theory. *International Journal of Mass Spectrometry and Ion Physics* **1975,** 17, (3), 309-319.

28. Shockley, W., Currents to conductors induced by a moving point charge. *Journal of Applied Physics* **1938,** 9, (10), 635-636.

29. Comisarow, M. B., Signal modeling for ion cyclotron resonance. *The Journal of Chemical Physics* **1978,** 69, (9), 4097-4104.

30. Campuzano, I.; Bush, M. F.; Robinson, C. V.; Beaumont, C.; Richardson, K.; Kim, H.; Kim, H. I., Structural characterization of drug-like compounds by ion mobility mass spectrometry: comparison of theoretical and experimentally derived nitrogen collision cross sections. *Analytical chemistry* **2012,** 84, (2), 1026-1033.

31. Bush, M. F.; Hall, Z.; Giles, K.; Hoyes, J.; Robinson, C. V.; Ruotolo, B. T., Collision cross sections of proteins and their complexes: a calibration framework and database for gas-phase structural biology. *Analytical chemistry* **2010,** 82, (22), 9557-9565.

32. Shelimov, K. B.; Clemmer, D. E.; Hudgins, R. R.; Jarrold, M. F., Protein structure in vacuo: Gas-phase conformations of BPTI and cytochrome c. *Journal of the American Chemical Society* **1997,** 119, (9), 2240-2248.

33. Valentine, S. J.; Counterman, A. E.; Clemmer, D. E., Conformer-dependent proton-transfer reactions of ubiquitin ions. *Journal of the American Society for Mass Spectrometry* **1997,** 8, (9), 954-961.

34. Leach Iii, F. E.; Kharchenko, A.; Heeren, R.; Nikolaev, E.; Amster, I. J., Comparison of particle-in-cell simulations with experimentally observed frequency shifts between ions of the same mass-to-charge in Fourier transform ion cyclotron resonance mass spectrometry. *Journal of the American Society for*

Mass Spectrometry **2010,** 21, (2), 203-208.

35. Tinkle, M. D.; Barlow, S. E., Image charge forces inside conducting boundaries. *Journal of Applied Physics* **2001,** 90, (3), 1612-1624.

36. Kuhnen, F.; Wanczek, K. P., Investigation of the ion movement in open ICR cells with computer simulations. *International journal of mass spectrometry and ion processes* **1998,** 173, (1), 81-90.

37. March, R. E.; Todd, J. F. J., *Quadrupole Ion Trap Mass Spectrometry*. 2nd edition ed.; John Wiley & Sons Inc.: Hoboken, New Jersey, 2005.

Table 1

Table 1. Typical ion kinetic energy in the laboratory reference frame, maximum exchange energy available and mean free path inside the FT-ICR cell used in this study. Buffer gas N_2.

Name	***Cytochrome C***	***Ubiquitin***	***Angiotensin I***	***MRFA***
Mass (amu)	~12369	~8570	1295.6	522.5
Charge	+15	+10	+3	+1
m/z	~825	~857	433	~524
KE (ev)	~27000	~17500	~10400	~2870
Maximum exchange energy (ev)	~123	~114	~440	~291
CCS ($Å^2$)	~2579	~1732	~474	~160
Mean free path at 10^{-10} Torr (km)	~12	~18	~66	~194

Note: CCS for cytochrome C, ubiquitin and angiotensin I was taken from ref [32], ref[33] and ref[31], respectively; CCS for MRFA was the calculated value from this study.

Figure 1

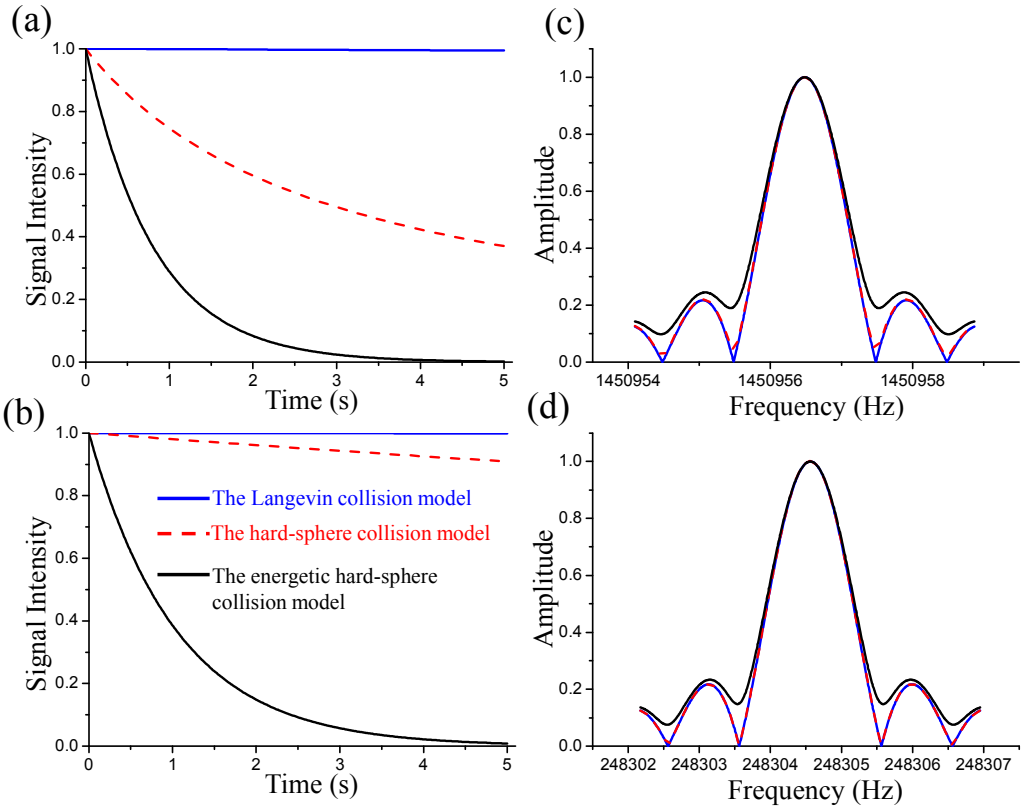

Figure 1. Image current decay curves of (a) tetramethylammonium (m/z 74.1, hard-sphere CCS 107.4 $Å^2$) and (b) angiotensin I (m/z 433, hard-sphere collision cross section 474 $Å^2$) using different collision models. The corresponding frequency-domain spectra of (c) tetramethylammonium and (d) angiotensin I. Buffer gas N_2, pressure $2 * 10^{-10}$ Torr, magnetic field strength 7 T, ion cyclotron radius 20 mm.

Figure 2

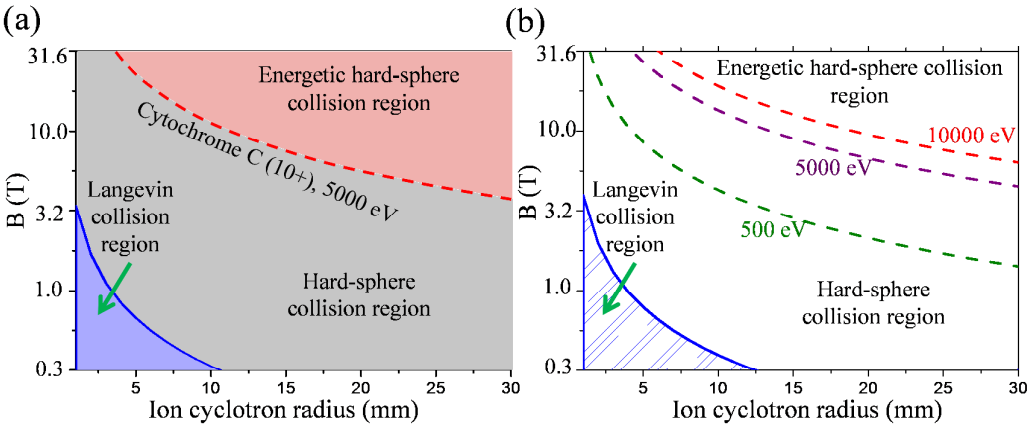

Figure 2. Suitable application regions of different collision models. (a) The suitable application regions of different collision models for cytochrome C. Threshold *KE* is assumed to be 5000 eV (see text for details). (b) Effects of the threshold *KE* for ubiquitin ions (7+). Buffer gas N_2, pressure $2 * 10^{-10}$ Torr. Note: y-axis was plotted in Log scale.

Figure 3

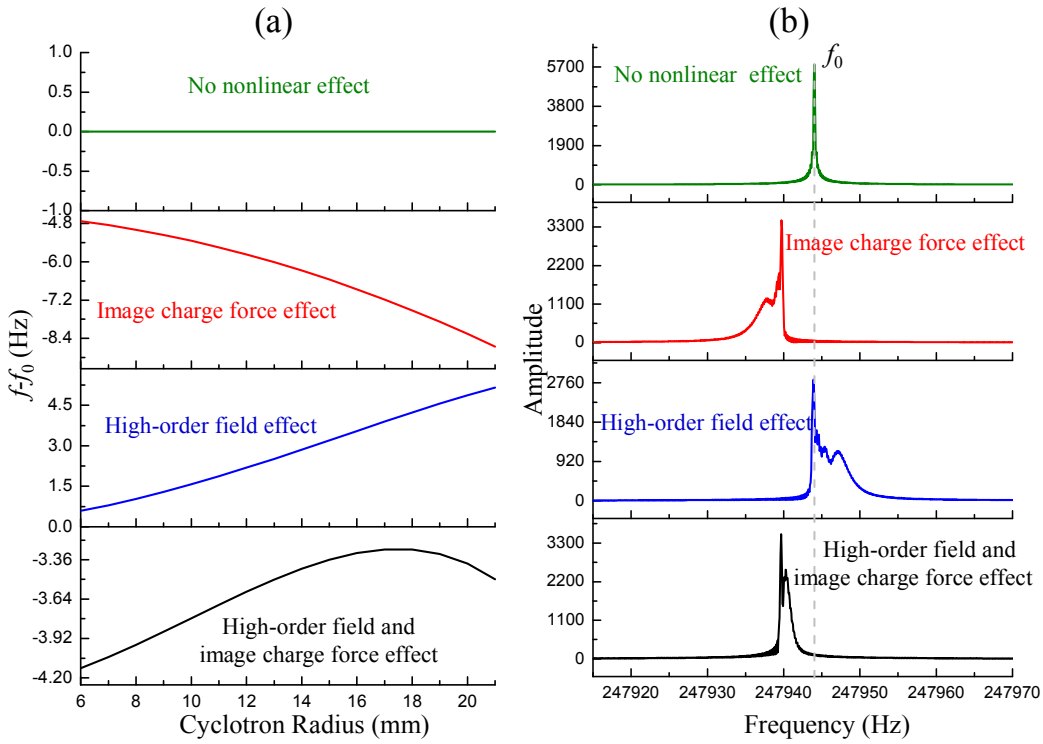

Figure 3. Nonlinear effects caused by high-order electric fields and image charge forces. (a) Ion cyclotron frequency shift along with ion cyclotron radius. (b) The corresponding frequency domain spectra. A 5-second-long time domain signal was used when performing FFT. m/z = 433, z = 3, hard-sphere CCS 474 Å^2, buffer gas N_2, pressure 5 * 10^{-9} Torr, Trapping voltage 2 V. The high-order fields contain -20% octopole field and 10% dodecapole field. The image charge force is induced by 1.2*10^6 ions within an infinite long cylindrical ICR cell.

Figure 4

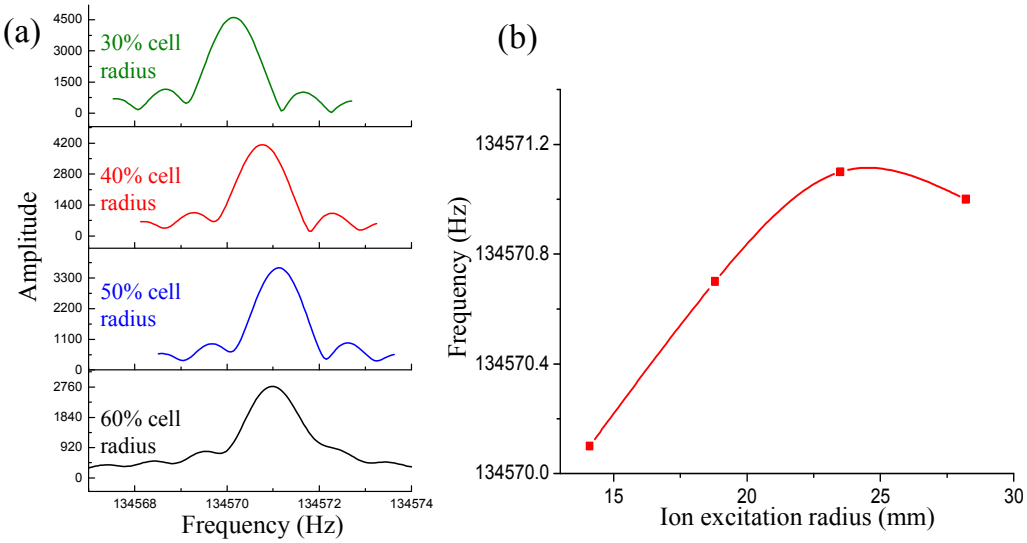

Figure 4. Measured ion cyclotron frequencies at different cyclotron radiuses, ubiquitin (8+). (a) peak shape; (b) center frequency shifts.

Figure 5

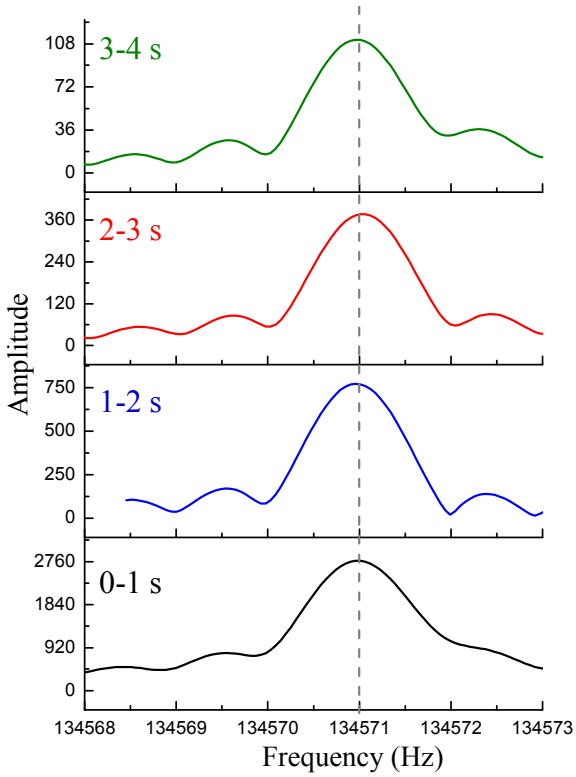

Figure 5. The spectra of ubiquitin at different periods of time. Ion excitation radius 28.2 mm (60% cell radius).

TOC

An energetic hard-sphere collision model for modern high-resolution FT-ICR.